Kufa Journal of Engineering
Vol. 17, No. 3, July 2026, P.P. 136-160
Article history: Received 15 May 2025, last revised 19 July 2025, accepted 26 August 2025

IMPROVING PHYSICAL PROPERTIES (DENSITY, POROSITY, WETTABILITY, AND YOUNG'S MODULUS) OF TITANIUM METAL THROUGH SMALL LIQUID METAL GALLIUM ADDITIONS FABRICATED BY POWDER METALLURGY FOR BIOMEDICAL APPLICATIONS

Ammar Razzaq Hasan[1,2], Emad S. Al-hassani[3], and Fatimah J. Al-Hasani[4]

[1] University of Technology, Materials Engineering Department, Baghdad, Iraq, Email:ammarr.Alshemary@uokufa.edu.iq.

[2] University of Kufa, Faculty of Engineering, Materials Engineering Department, Najaf, Iraq.

[3] University of Technology, Materials Engineering Department, Baghdad, Iraq, Email:emad.S.Alhassani@uotechnology.edu.iq.

[4] University of Technology, Materials Engineering Department, Baghdad, Iraq, Email:fatimah.J.Alhasani@uotechnology.edu.iq.

https://doi.org/10.30572/2018/kje/170309

ABSTRACT

This study investigates the influence of liquid metal ga additions (1-2.5 wt%) on the structural, physical, and biological properties of ti metal, which are fabricated by the powder metallurgy method. The alloys were manufactured by sintering at 1250 °c to improve the metallic implants for biotribological applications. Xrd, sem and edx analyses were used to identify the predominant compounds and phases before and after gallium addition. The structural examination by xrd and sem showed an improvement in the crystal structure distribution and a phase transformation, with a significantly smaller grain size due to the increased gallium content. A change in the proportions of the predominant phases was observed, with the appearance of intermetallic compounds $tiga_3$ and ti_3ga. The density, porosity, wettability, and young's modulus were also tested. The results indicate a decrease in the density, wettability, and young's modulus of the samples at different concentrations and an increase in the porosity of the samples with the lowest density occurring at 1% ga, attributed to the formation of a disordered solid solution with decreased atomic packing efficiency, which reduces the density overall. This resulting in increased porosity due to incomplete densification during sintering. In addition, ga reacts with ti at higher ga concentrations to form an intermetallic compound $tiga_3$ and ti_3ga, through metal bonding. This intermetallic compound forms a chemically compatible interface, thereby reducing the contact angle and enhancing wettability. The low young's modulus of the samples is due to the very low young's modulus of ga, about (9.8 gpa), and to distortion of the crystal lattice, increased atomic void volume, and the formation of weakly bonded intermetallic compounds. Finally, cytotoxicity and biocompatibility tests were performed on the samples. The results showed low cytotoxicity to mcf-10 at concentrations of up to 50 µg/ml for all samples, and this gradually increased with higher concentrations up to 100 µg/ml, due to the potential release of gallium ions. The increase in gallium led to increased cytotoxicity, but it remained within acceptable limits. This makes all samples promising candidates for biomaterials applications.

KEYWORDS

Gallium, titanium, powder metallurgy, density, porosity, wettability, young’s modulus, biomaterial.

1. INTRODUCTION

Titanium and its alloys have been used among the most extensively in the biomedical field due to their excellent biocompatibility, mechanical properties, antibacterial properties, and corrosion resistance (Sarraf et al., 2022). In addition, Titanium and its alloys have an elastic modulus lower than conventional biomaterials such as stainless steel and cobalt-chromium alloys (Jasim et al., 2020). Furthermore, titanium and its alloys have been shown to promote bone growth and osseointegration in implant applications (Alipal et al., 2021). While titanium and its alloys have many advantages in biological environments, they also have some disadvantages that limit their use in certain applications (Sidhu et al., 2021). Titanium and its alloys are characterized by high density, which can increase the weight and size of the implant, affecting patient movement and comfort (Naghavi et al., 2023). They also have a high Young's modulus, which can cause stress shielding, bone resorption, and loosening of the implant due to its incompatibility with natural tissues (Abbass et al., 2021). However, the addition of pure metals to titanium and its alloys is a common approach to improve their physical and biological properties. By adding specific metals, it is possible to tailor the properties of titanium and its alloys to meet specific application requirements (Abbass et al., 2020). In recent years, there has been significant research and development aimed at improving the properties and applications of these materials in the medical industry (Jiang et al., 2023). Titanium and its alloys have a wide range of applications in the human body, including dental implants, orthopedic implants, and cardiovascular devices (Jasim et al., 2020). Several studies have reported that the addition of Ga to titanium and its alloys can improve their mechanical and physical properties.

(Zhu et al., 2023) developed A new Ti-8Al-1Cr-1V-0.5Fe-0.1Si (wt.%) alloy with a low-density and high-strength in this work. Lightweight titanium alloys are achieved by substituting heavy elements (Mo, V) with aluminum, reducing density while maintaining strength. This newly developed alloy is a potential material for various structural applications.

(Alberta et al., 2023) investigated the tribo-electrochemical behavior of two β-type (100-x) (Ti-45Nb)-XGa (x = 4, 8 wt. %) alloys, along with β-Ti-45Nb and medical grade Ti-6Al-4V ELI, in a physiological solution. The research evaluated the microstructure and mechanical behavior of the alloys by X-ray diffraction, microhardness, and ultrasonic method. The research also evaluated the tribocorrosion behavior of the alloys by potentiodynamic polarization, electrochemical impedance spectroscopy, and wear tests. The research found that the addition of Ga to Ti-Nb alloys improves their corrosion resistance and reduces their wear rate in a physiological solution. The research also found that the tribocorrosion performance of the Ti-Nb-Ga alloys is comparable or superior to that of Ti-6Al-4V ELI.

(Fortouna et al., 2023) investigated the influence of Ga additions (2, 4, 6, and 8 wt. %) on the microstructure, mechanical behavior, and electronic properties of β-Ti-45Nb alloy by a combination of experiments and density functional theory (DFT). The research prepared the alloys by melting arc and characterized them by using X-ray diffraction, scanning electron microscopy, energy-dispersive spectroscopy, transmission electron microscopy, Vickers hardness test, tensile test, and electrochemical impedance spectroscopy. The research also performed DFT calculations to analyze the electronic structure and elastic constants of the alloys. The research found that the Ga additions do not affect the single β-phase microstructure of the alloys but increase their lattice parameter and density. The research also found that the Ga additions improve the hardness, strength, ductility, corrosion resistance, and biocompatibility of the alloys, as well as their elastic anisotropy and ductility index.

(Vishnu et al., 2022) prepared three novel β-type (Ti–45Nb)-based alloys with minor additions of the antibacterial elements Ga and Cu $(Ti\text{-}45Nb)_{96}$-4Ga, $(Ti\text{-}45Nb)_{96}$-4Cu and $(Ti\text{-}45Nb)_{96}$-2Ga-2Cu wt.%) by a two-step casting process followed by homogenization treatment. The research characterized the microstructure, phase composition, mechanical properties, corrosion behavior, and antibacterial activity of the alloys. The research found that the Ga and Cu additions refine the grain size and increase the fraction of β phase in the alloys. The research also found that the Ga and Cu additions improve the antibacterial activity of the alloys but reduce their strength and modulus.

(Cochis et al., 2019) evaluated the antibacterial activity and biocompatibility of titanium alloys with metallurgical additions of gallium (Ga), which is a metal that can replace iron in bacterial metabolism and inhibit their growth. The research prepared Ti–6Al–4V alloys with different Ga contents (1, 2, 20, and 23 wt. %) by vacuum arc melting and characterized their microstructure, mechanical properties, and corrosion behavior. The research also tested the antibacterial activity of the alloys against Staphylococcus aureus and Escherichia coli, as well as their cytotoxicity on human osteoblasts and fibroblasts. The research found that the Ga addition does not affect the microstructure and mechanical properties of the alloys but slightly increases their corrosion rate. The research also found that the Ga addition confers a strong time-increasing antibacterial activity to the alloys, without any cellular toxicity.

This research distinguishes itself from previous research by utilizing a powder metallurgy manufacturing method that combines solid titanium powder with liquid gallium metal. Powder metallurgy technology is characterized by its ability to manufacture alloys and components with high efficiency, precision, and flexibility, especially for complex shapes and customized material properties. Its advantages in material utilization, design flexibility, and the ability to produce unique materials make it a critical technology in modern manufacturing, especially in high-volume and advanced applications.

To improve titanium's performance in medical applications, the density and Young's modulus must be reduced by adding liquid gallium metal.

2. MATERIALS AND METHODS

2.1. Materials used

Pure titanium is a lustrous transition metal with a silver color, low density, and high strength. It is resistant to corrosion in seawater and chlorine. The titanium used is a powder with a purity of up to 99.8% imported from Fluka Company (brand name of Honeywell Research Chemicals) in Morris Plains, New Jersey, USA.

Pure gallium is a silvery blue metal that fractures conchoidally like glass. It also has a very low melting point of 29.76 °C (85.57 °F). The gallium used is a liquid metal with a purity of up to 99.9% imported from Fluka Chemie GmbH in Buchs, Switzerland.

2.2. Preparation of samples by powder metallurgy

Adding liquid metal Gallium (Ga) to metal powder (Ti) by mixing the powder and Gallium (Ga) in a mixing machine according to the following mixing process conditions as shown in Table 1.

Table 1 Processing conditions for mixing

Parameter	Condition
Mixing time	3hr
Rotation speed	100 rpm
Ball to powder ratio	4:1
Ball size and type	5mm-10mm \ Tungsten Carbide
Container size and type	1000 ml \ Tungsten Carbide

Adding liquid metal Gallium (Ga) to the metal powder (Ti) was prepared according to the following proportions and weights as shown in Table 2.

Table 2 Proportions and weights of metal powder Ti with (Ga)

According to			**Ti**		
Proportions (%)	100	99	98.5	98	97.5
Weights (gm)	20	19.8	19.7	19.6	19.5
According to			**Ga**		
Proportions (%)	0	1	1.5	2	2.5
Weights (gm)	0	0.2	0.3	0.4	0.5
According to			**Ti-XGa**		
Proportions (%)	100	100	100	100	100
Weights (gm)	20	20	20	20	20

After adding liquid metal Gallium (Ga) to alloy powder, Alloy powder annealing at room temperature and sunlight to increase the chemical reaction between gallium liquid metal and Ti powder under the following conditions as shown on Table 3.

Table 3 Annealing conditions

Parameter	Condition
Time	(5-7) days
Temperature	(35-45) ºC

Then weight the quantity of powders used for each sample; Through the size of the sample to be manufactured and the density of the powder, the weight of the powder can be determined. The weight of powders used for each sample as shown in Table 4.

Table 4 Weight the quantity of powders used for each sample

Size	Weight
(10*5) mm^2	1.76 g
(15*7) mm^2	5.56 g
(30*3) mm^2	9.54 g

Then weight the required quantity of powder; lubricate the mold (die) and fill the die cavities with the required quantity of powder.

Alloy Powder pressing (compaction) by using hydraulic press machine under the following conditions as shown in Table 5 to obtain the required compact density of the samples.

Table 5 Pressing conditions

Parameter	Condition
Compaction load (ton)	20
Time hold (min)	5

Then, compact (Green parts) anneal at room temperature and sunlight to complete the chemical reaction between gallium metal and other elements in the green parts. Under the conditions shown in Table 3.

Green parts (Compact) sintering at argon gas tube furnace type (GSL-1500X), Argon is nonflammable and inert used to a back fill in furnace under the following conditions as shown in Table 6. The reason for sintering at stepped temperatures before the high hold grade to removal of the pressing lubricant and Preventing cracking due to expansion and thermal shock.

Table 6 Sintering conditions

Parameter	Temperature (ºC)	Time (hold) (min)
Step$_1$Temperature	250	15
Step$_2$ Temperature	500	15
Sintering Temperature	1250	90-120

Then prepare the samples for examination by Grinding their surfaces using Grind paper (100, 180, 240, 320, 400, 600, 800, 1000, 1200). Fig. 1 shows the shape of the samples after the Grinding process.

Fig. 1 shows the shape of the samples after the Grinding process

Final samples were manufactured according to different gallium percentages as shown in Table7.

Table 7 Final manufactured samples

Sample No.	Ti-XGa
Sample 1	Ti
Sample 2	Ti-1Ga
Sample 3	Ti-1.5Ga
Sample 4	Ti-2Ga
Sample 5	Ti-2.5Ga

2.3. Samples examination

2.3.1. Characterization

X-ray diffraction (XRD) testing of the samples was performed using an XRD device manufactured by Thermo Scientific, USA. Scanning electron microscopy (SEM) testing was conducted on the samples using a SEM device manufactured by Thermo Scientific, USA. Finally, Energy-Dispersive X-ray Spectroscopy (EDX) testing was performed on the samples using an EDX device manufactured by Shimadzu, Japan.

2.3.2. Density Test

In general, the density achieved in sintered products is between 70% and 95 % of the fully dense wrought products, depending on the production technology in use and the type of application.

To find the density of metal alloys, several established methods can be employed. The most common techniques include the oil impregnation method.

The test steps are explained as follows:

1- Dry the samples at 100°C for two hours and take dry weight.

2- Put the samples in oil with a density of 0.8, then withdraw the oil into the samples to fill the pores using the vacuum process for 30 min.

3- Weighing wet weight and then the suspended weight and extracting the density using a balance that supports calculating the density according to Archimedes' principle.

The apparent density of the alloy, denoted as ρ, is determined through the oil impregnation method, according to (ISO standard 2738).

The formula being:

$$\rho = \frac{A}{B - C} = g/cm^3 \quad (1)$$

Where:

ρ is the apparent density (g/cm^3).

A is the weight of the unimpregnated part in air (dry weight), gm.

B is the weight of the part after impregnating with the oil (wet weight), gm.

C is the mass of the impregnated part in water (suspended weight), gm.

2.3.3. Porosity Test

The amount of interconnected porosity (p in %) can be calculated as follows:

$$p = \frac{\rho^{\circ} - \rho}{\rho^{\circ}} \times 100\% \quad (2)$$

Where:

p is the porosity (%).

ρ is the apparent density (g/cm^3).

ρ° is the theoretical density (g/cm^3).

The theoretical density of the alloy can be calculated by using the formula:

$$\rho^{\circ} = m_1 \rho^{\circ}{}_1 + m_2 \rho^{\circ}{}_2 \quad (3)$$

Where:

ρ° is the theoretical density (g/cm^3).

m_1 and m_2 are the weight fractions of elements 1and 2.

$\rho^{\circ}{}_1$ and $\rho^{\circ}{}_2$ are the theoretical density of elements 1and 2.

2.3.4. Wettability (Contact Angle) Test

The wettability (contact angle) of the samples was tested using the sessile drop technique with distilled water by using Optical Contact Angle and Interface Tension Meter, model SL200KS (developed by USA KINO) manufactured by Solon Tech, in Shanghai, China, found in Ceramic Department /Materials Engineering College/ University of Babylon. This procedure involved dropping 1 µml of distilled water on the sample surface and measuring the contact angle of the water every 10 seconds. The contact angle was measured ten times for each sample by both the Circular Fitting and Young-Laplace Fitting methods. The Circuit Fitting method has been adopted as the most widely used method for calculating the contact angle due to its high accuracy.

2.3.5. Elastic Modulus Calculate Test

The elastic modulus was found by generating ultrasound pulses, both longitudinal and transverse, in cylindrical samples by using (Ultrasonic type CCT-4 UK Tester) and solving the following equations:

$$\boldsymbol{\mathcal{V}} = \mathbf{1} - \frac{\mathbf{1}}{\mathbf{2}} \times \frac{\mathbf{1}}{\mathbf{1} - (\boldsymbol{C}_{\mathbf{trans}}/\boldsymbol{C}_{\mathbf{long}})^{\mathbf{2}}} \quad (4)$$

$$\boldsymbol{E} = 2 \times \boldsymbol{\rho} \times (\mathbf{1} + \boldsymbol{\mathcal{V}})(\boldsymbol{C}_{\mathbf{trans}})^{\mathbf{2}} \quad (5)$$

Where:

C_{trans} is the transverse wave speed.

C_{long} is the longitudinal wave speed.

$\mathcal{V}$ is Poisson's ratio.

E is Young's modulus (modules of elasticity).

ρ is the density of the material (the density value assumes an isotropic, homogeneous, and nondispersive material). The device used Concrete Tester type cct-4 Microseconds manufactured by CSI - Contractors Supply Inc, which is found in the Ceramic Department /Materials Engineering College/ University of Babylon.

2.3.6. MTT assay (Cytotoxicity assay)

Maintenance of cell cultures: The MCF-10 cell line was cultured in RPMI-1640 enriched with 10% fetal bovine serum, 100 units/mL penicillin, and 100 µg/mL streptomycin. Cells were subcultured using trypsin-EDTA, reseeded at 80% confluence biweekly, and incubated at 37 °C. The MTT assay was conducted using 96-well plates to evaluate the cytotoxic effect of sample 3, which possesses superior mechanical properties. Cell lines were inoculated at a density of 1×10^4 cells per well after 24 hours. Alternatively, a confluent monolayer was established, and MCF-10 cells were subjected to treatment with sample 3. Cell viability was assessed after 72 hours of treatment by discarding the medium, introducing 100 µL of 2 mg/mL MTT, and incubating the cells for 2.5 hours at 37 °C. After the removal of the MTT solution, the crystals in the wells were solubilized by the addition of 130 µL of DMSO (Dimethyl Sulphoxide), followed by a 15-minute incubation at 37 °C with agitation. The absorbance was measured using a microplate reader at 492 nm; the test was conducted in triplicate. The cell growth inhibition rate (cytotoxicity percentage) was determined using the subsequent equation:

$$\mathbf{Inhibition\ rate}\ (\mathbf{Cytotoxicty}\ \%) = \frac{\boldsymbol{A}-\boldsymbol{B}}{\boldsymbol{A}} \times \mathbf{100} \quad (6)$$

Where:

A is the absorbance of control.

B is the absorbance of the tested sample.

The obtained data were statically analyzed using an unpaired t-test with GraphPad Prism 10. The values were presented as the mean ± SD of triplicate measurements.

3. RESULTS

3.1. XRD test results

The XRD data and the Rietveld refinement, based on XRD patterns of (Ti-XGa) using (Rietveld purification), and (FullProf) software, confirmed the dominance of α-Ti phase (HCP) structure in all Ga-containing samples, with detectable formation of intermetallic compounds at concentrations ≥1 wt.%. The progressive shift in α peaks and changes in lattice constants suggest Ga incorporation into the Ti lattice until saturation. The atomic radius of Ti is 147 picometers (pm) or 1.47 angstroms (A°), while the atomic radius of Ga (135 pm) or (1.35 A°). This structural evolution may correlate with observed changes in mechanical and antibacterial behavior.

However, when gallium is added to titanium, it primarily lowers the α to β phase transition temperature (223 °C). Gallium is not classified as an α or β phase stabilizer in pure titanium, but rather as a structural modifier that leads to intermetallic compounds Ti_3Ga and $TiGa_3$ at high concentrations. As in Fig. 2.

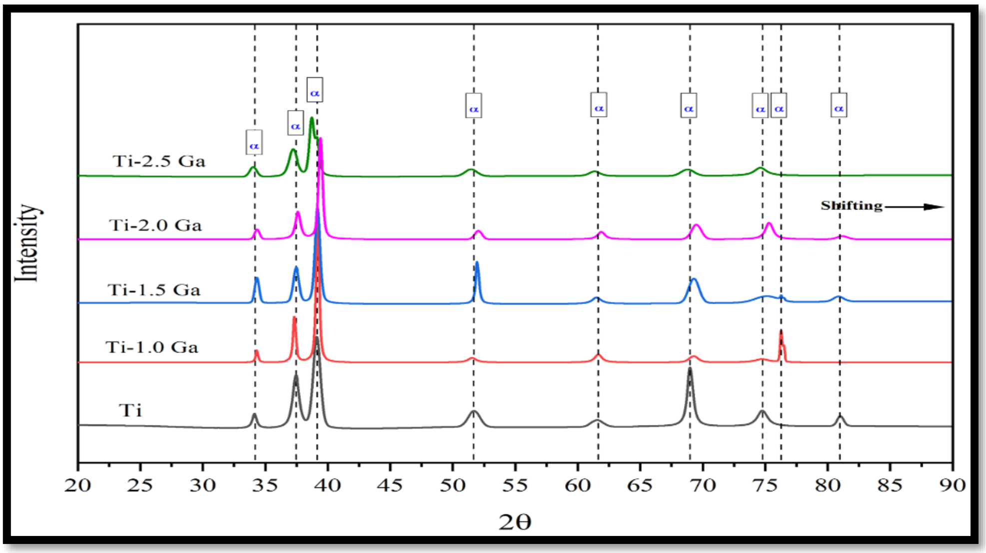

Fig. 2 XRD pattern for Ti-xga

The Rietveld refinement analysis on the XRD pattern of commercially pure titanium (CP-Ti) confirmed that the examined titanium sample consists exclusively of α-Ti phase with hexagonal close-packed (HCP) crystal structure (100%). No evidence of β-Ti, oxide phases or intermetallic compounds were detected, confirming high phase purity with crystallite size (~90-100 nm). As in Fig. 3.

The Rietveld refinement on the XRD pattern of Ti-1Ga alloy confirmed the dominance of α-Ti phase in the Ti-1Ga alloy (~97-98%), with only minor presence of Ti_3Ga intermetallic compound (~2-3%), likely due to limited Ga solubility in the HCP matrix. Lattice parameters slightly decreased compared to pure Ti, with crystallite size (~85-90 nm). As in Fig. 4.

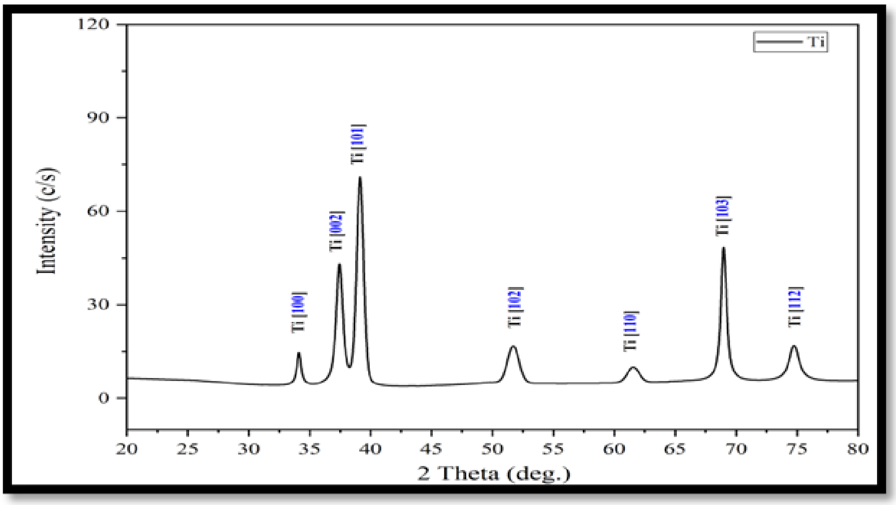

Fig. 3 XRD pattern for Sample 1

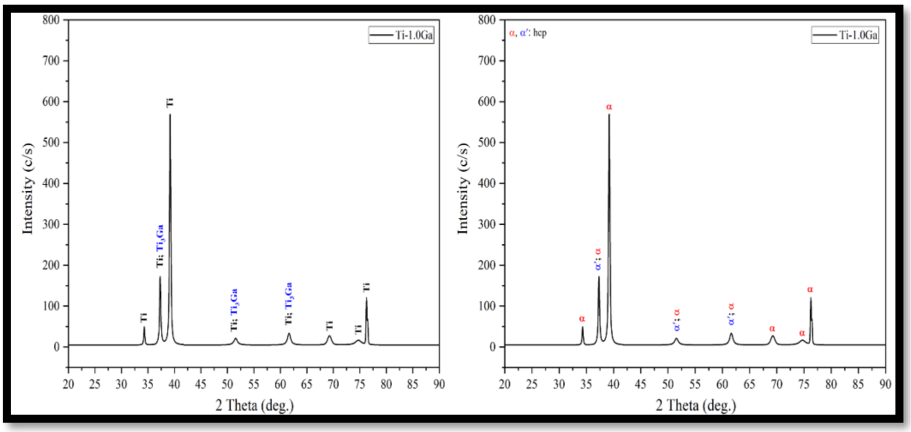

Fig. 4 XRD pattern for Sample 2

Rietveld refinement on the XRD pattern of the Ti-1.5Ga sample revealed a predominant α-Ti phase (~94%), along with the Ti_3Ga intermetallic compound (~6%). The shift in the peaks indicates lattice contraction due to gallium intrusion into the titanium crystal lattice, with crystallite size (~80-85 nm). The appearance of Ti_3Ga also reflects the onset of solid solubility saturation of gallium in the α phase, which impacts the mechanical and biological properties of the alloy. As in Fig. 5.

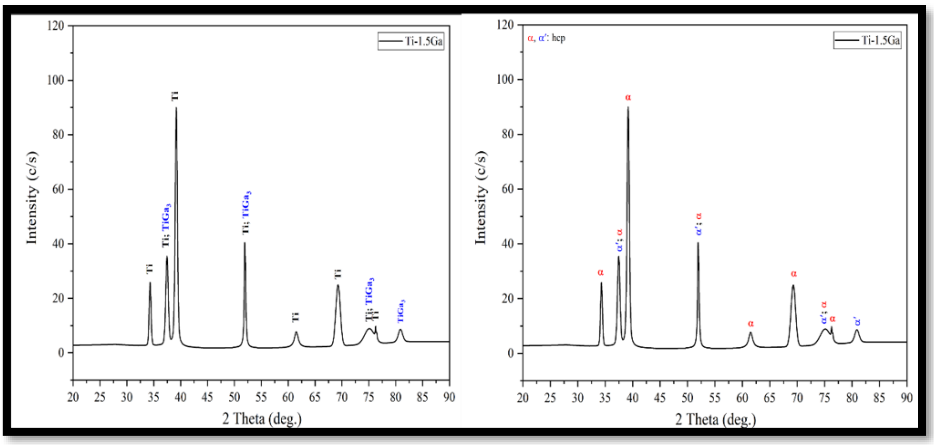

Fig. 5 XRD pattern for Sample 3

Rietveld analysis on the XRD pattern of the Ti-2Ga sample showed that adding 2% gallium to pure titanium results in a (~10%) Ti_3Ga intermetallic compound, with the α-Ti phase still dominating (~90%), with crystallite size (~78 nm). The introduction of gallium resulted in a slight contraction of the lattice constants due to its substitution at the titanium atomic sites. These structural changes reflect the onset of solid solubility saturation and support the hypothesis that gallium influences the formation of new phases and the potential improvement of the alloy's mechanical and biological properties. As in Fig. 6.

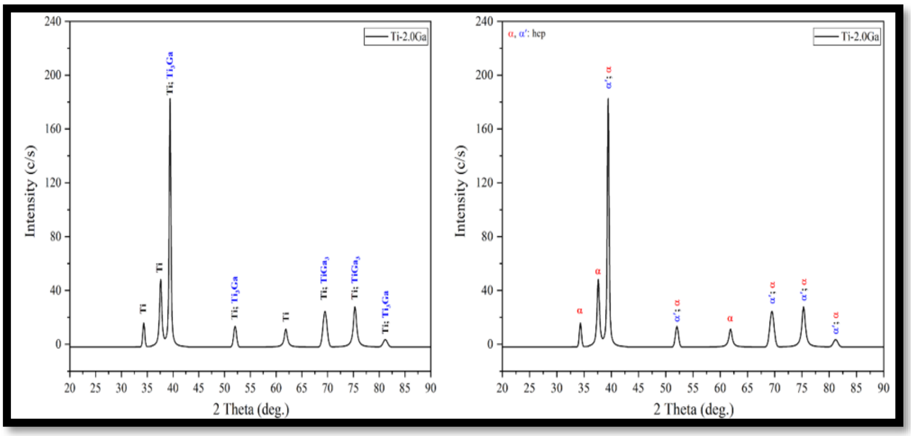

Fig. 6 XRD pattern for Sample 4

Rietveld refinement results on the XRD pattern of the Ti-2.5Ga sample showed that the dominant phase is still α-Ti at (~86%), but with a marked increase in the proportion of intermetallic compounds Ti_3Ga (~9%) and $TiGa_3$ (~5%), with crystallite size (~75 nm). This indicates that gallium exceeds the solid solubility of the α-phase and forms as independent compounds at this proportion. The change in lattice constants also supports the hypothesis of partial replacement of gallium within the titanium lattice. These structural changes are expected to affect the mechanical performance and dynamic behavior of the alloy. As in Fig. 7.

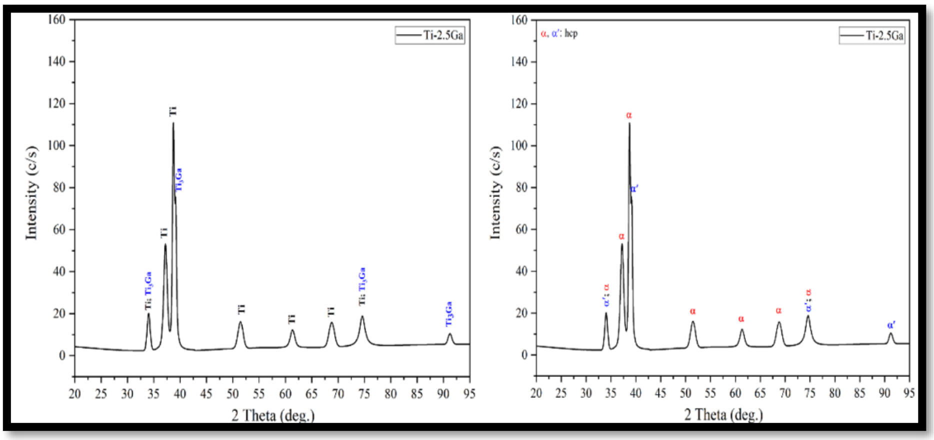

Fig. 7 XRD pattern for Sample 5

3.2. SEM test results

SEM images indicate that the main phase of the Ti metal was the α phase. Adding liquid gallium metal in small proportions enhances the stability of the α-phase, in addition to the appearance of intermetallic compounds Ti_3Ga and $TiGa_3$.

Fig. 8 shows the α-Ti (Single Phase-Grains). This phase represents the only structure present in the sample and appears as clear crystalline grains. The separated regions represent the titanium crystal grains, which fall into only one phase: α-Ti (HCP hexagonal structure).

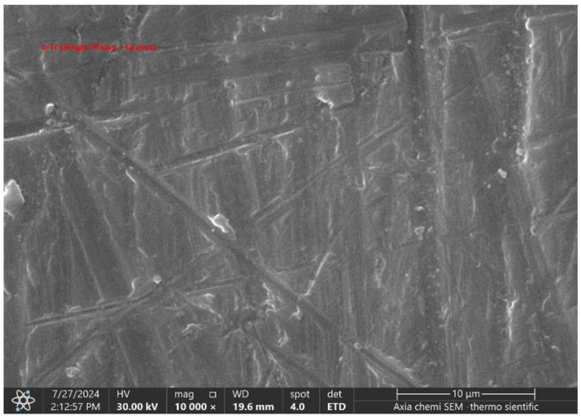

Fig. 8 SEM image for Ti metal

Fig. 9 shows that α-Ti (Matrix), the primary titanium phase, forms most of the structure, and Ti_3Ga is an intermetallic compound formed by adding gallium, often present as particles or regions of varying contrast. Areas with a uniform color (light gray) represent the α-Ti phase, the primary phase of the metal. Structures appeared with different contrast (brighter or darker spots or areas) that represented the Ti_3Ga intermetallic compound, resulting from the reaction of gallium with titanium.

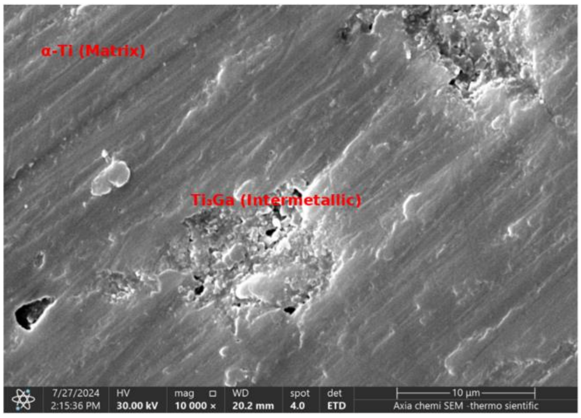

Fig. 9 SEM image for Ti-1Ga alloy

Fig. 10 shows the α-Ti (Matrix), the primary phase of titanium, forming the homogeneous gray background. Ti_3Ga/Ti_2Ga intermetallic compounds are more visible here due to the increased gallium concentration. They are often found at grain boundaries or as fine particles-regular gray areas α-Ti phase (Primary titanium). Areas marked by different contrasts or the appearance of fine particles Ti_3Ga or Ti_2Ga compounds are more pronounced here than the Ti-1Ga sample due to the increased gallium concentration.

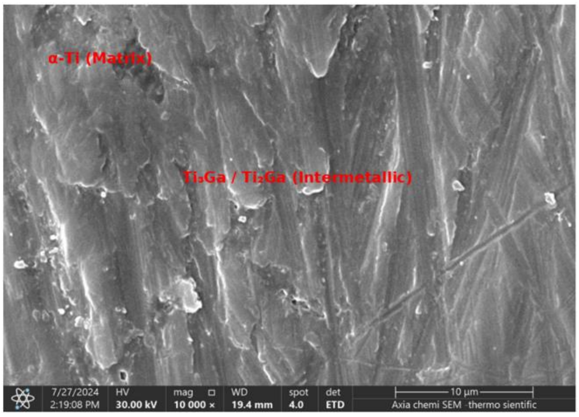

Fig. 10 SEM image for Ti-1.5Ga alloy

Fig. 11 shows the α-Ti (Matrix), the primary phase that forms the overall structure of the mineral. Ti_3Ga/Ti_2Ga intermetallic compounds that become more pronounced at this concentration are often distributed at grain boundaries or as fine particles within the structure. Regular gray areas represent the α-Ti phase. High-contrast areas (spots or prominent lines) indicate the presence of intermetallic compounds such as Ti_3Ga and Ti_2Ga, which become more pronounced with increasing gallium content.

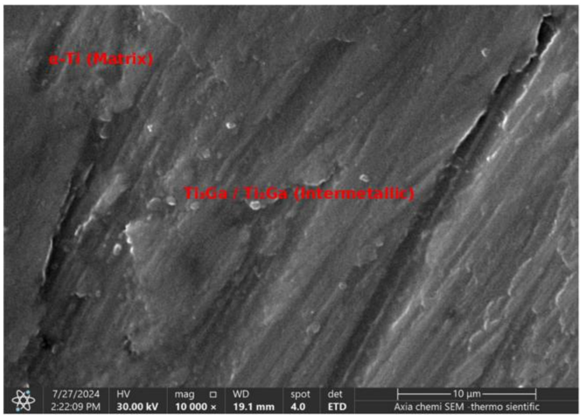

Fig. 11 image Test for Ti-2Ga alloy

Fig.12 shows the α-Ti (Matrix), the primary phase of titanium, representing the overall structure. Ti_3Ga/Ti_2Ga Intermetallic compounds become more pronounced and denser at this gallium concentration, often appearing as prominent or contrasting spots in the image. Uniform gray areas represent the α-Ti phase clear contrasts (bright or dark spots) indicate intermetallic compounds such as Ti_3Ga and Ti_2Ga, which are denser and more pronounced at this high gallium concentration.

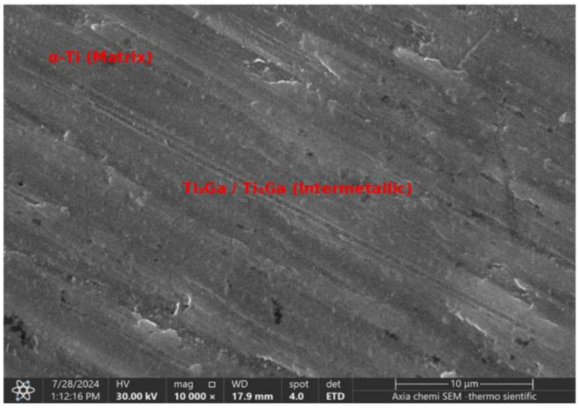

Fig. 12 SEM image for Ti-2.5Ga alloy

3.3. EDX test results

EDX data indicates the proportions of metallic elements present in the Ti metal before and after adding liquid gallium metal at proportions (1%, 1.5%, 2%, and 2.5%) as in Fig. 13 and 14.

Quantitative Result

Analyte	Result	
Ti	99.765	%
Al	0.070	%
Si	0.055	%
Ca	0.054	%
Fe	0.051	%
Cu	0.026	%
Zn	0.008	%

Fig. 13 EDX for Ti metal

Quantitative Result

Analyte	Result	
Ti	98.708	%
Ga	0.942	%
Al	0.074	%
Si	0.066	%
Gd	0.060	%
Mo	0.046	%
Ca	0.044	%
Os	0.032	%
Cu	0.021	%
Zr	0.005	%

EDX Test Results for Ti-1Ga

Quantitative Result

Analyte	Result	
Ti	98.207	%
Ga	1.455	%
Al	0.080	%
Si	0.053	%
Fe	0.052	%
Ca	0.048	%
Mo	0.048	%
Os	0.033	%
Cu	0.024	%

EDX Test Results for Ti-1.5Ga

Quantitative Result

Analyte	Result	
Ti	97.660	%
Ga	1.910	%
Al	0.083	%
Si	0.078	%
Gd	0.072	%
Mo	0.052	%
Ca	0.050	%
Fe	0.047	%
Cu	0.020	%
Mn	0.019	%
Zr	0.010	%

EDX Test Results for Ti-2Ga

Quantitative Result

Analyte	Result	
Ti	97.315	%
Ga	2.348	%
Al	0.091	%
Si	0.062	%
Mo	0.052	%
Fe	0.050	%
Ca	0.044	%
Cu	0.027	%
Zr	0.010	%

EDX Test Results for Ti-2.5Ga

Fig. 14 EDX for Ti-xga alloys

3.4. Density test results

This dual-density behavior highlights the interplay between atomic substitution, phase stability, and microstructure, offering tunable properties for aerospace and biomedical applications. Table 8 and Fig. 15 show the effect of adding gallium to Titanium metal in proportions of 1%, 1.5%, 2%, and 2.5% by powder metallurgy method on density.

Table 8 shows the effect of adding Ga to Ti metal on density

Sample	Dry weight (gm)	Wet weight (gm)	Suspended weight (gm)	Density (g/cm^3)
Sample 1	1.5935	1.6389	1.2331	3.9268
Sample 2	1.2159	1.2419	0.9287	3.8821
Sample 3	1.7070	1.7428	1.3044	3.8937
Sample 4	1.6994	1.7555	1.3266	3.9622
Sample 5	1.7563	1.8186	1.3758	3.9667

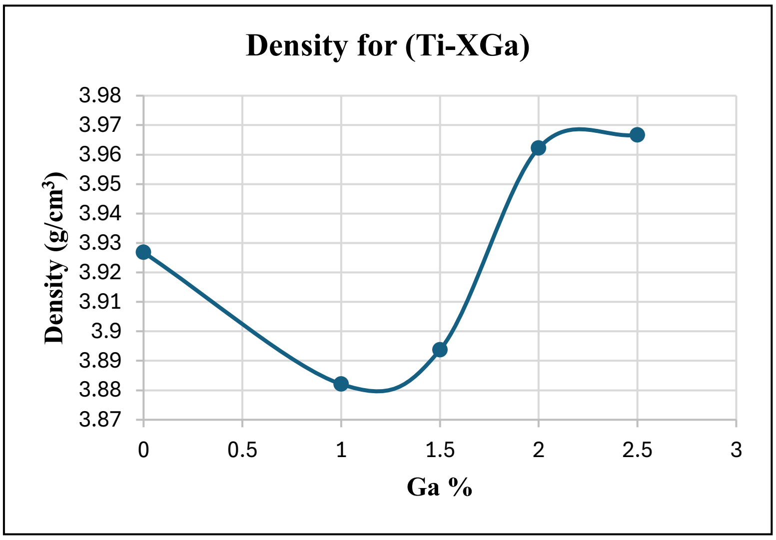

Fig. 15 shows the effect of adding Ga to Ti metal on density

3.5. Porosity test results

The dual porosity behavior in titanium and its alloys, modified with Ga, arises from atomic-level stress at low Ga and intermetallic densification at high Ga. This provides pathways to tailor porosity for aerospace (low porosity) or biomedical (controlled porosity) applications. Table 9 and Fig. 16 show the effect of adding gallium to Titanium metal in proportions of 1%, 1.5%, 2%, and 2.5% by powder metallurgy method on porosity.

Table 9 shows the effect of adding Ga to Ti metal on porosity

Sample	Theoretical density (g/cm^3)	Apparent density (g/cm^3)	Porosity %
Sample 1	4.506	3.9268	12.85
Sample 2	4.505	3.8821	13.87
Sample 3	4.521	3.8937	13.85
Sample 4	4.528	3.9622	12.58
Sample 5	4.535	3.9667	12.53

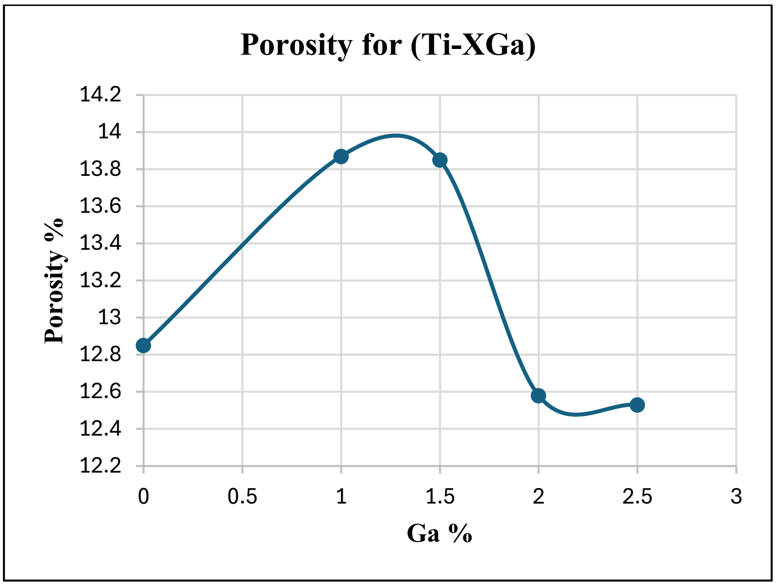

Fig. 16 shows the effect of adding Ga to Ti metal on porosity

3.6. Wettability (Contact Angle) test results

The dual wettability behavior of Ti-Ga systems arises from a balance between reactive bonding and interfacial degradation. Small Ga additions promote beneficial IMCs and oxide disruption, while high Ga concentrations trigger brittle phases and surface tension effects. Table 10 and Fig. 17 show the effect of adding gallium to Titanium metal in proportions of 1%, 1.5%, 2%, and 2.5% by powder metallurgy method on wettability.

Table 10 shows the effect of adding Ga to Ti metal on wettability

Time (s)		10	20	30	40	50	60	70	80	90	100
Sample 1	**Contact Angle (°)**	78.83	78.74	78.5	77.9	77.3	76.89	74.26	73.65	72.54	70.79
Sample 2		95.57	94.56	94.28	93.28	92.11	91.92	89.32	88.64	88.5	81.61
Sample 3		88.50	88	83.7	83.03	82.55	82.24	82.23	82	81.74	76.27
Sample 4		82.15	81.94	80.99	78.83	78.74	78.5	77.9	77.3	76.89	74.26
Sample 5		63.53	61.58	60.03	59.16	58.51	57.91	57.34	56.96	53.90	53.16

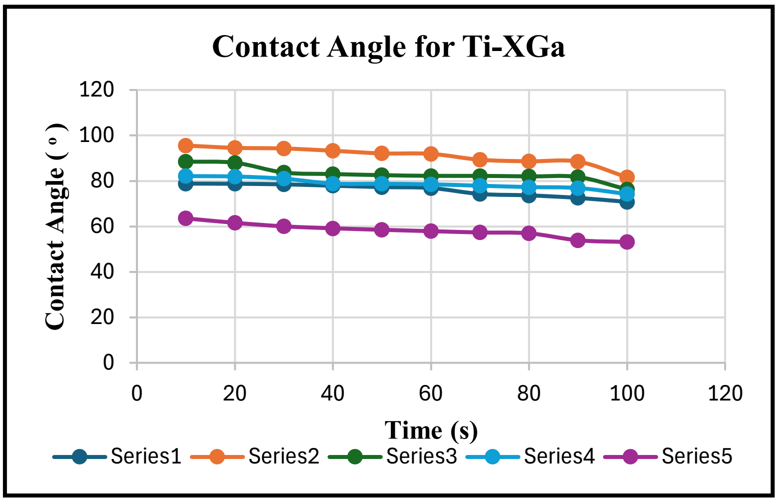

Fig. 17 shows the effect of adding Ga to Ti metal on wettability, when

(Series1= Sample 1, Series2= Sample 2, Series3= Sample 3, Series4= Sample 4, Series5= Sample 5)

3.7. Elastic Modulus Calculate Test Results

The reduced modulus of Ga-modified Ti alloys is advantageous for biomedical implants to matching Young's modulus of bone (~30 GPa) to prevent stress shielding. Table 11 and Fig. 18 show the effect of adding gallium to Titanium metal in proportions of 1%, 1.5%, 2%, and 2.5% by powder metallurgy method on Young's modulus.

Table 11 shows the effect of adding Ga to Ti metal on Young's modulus

Sample	Longitudinal wave speed (m/s)	Transverse wave speed (m/s)	Poisson's ratio	Density (g/cm^3)	Young's modulus (GPa)
Sample 1	3200	1000	0.445	3.9268	113.56
Sample 2	3180	950	0.451	3.8821	101.6
Sample 3	3150	900	0.456	3.8937	92
Sample 4	3100	880	0.456	3.9622	89.36
Sample 5	3050	880	0.454	3.9667	89.25

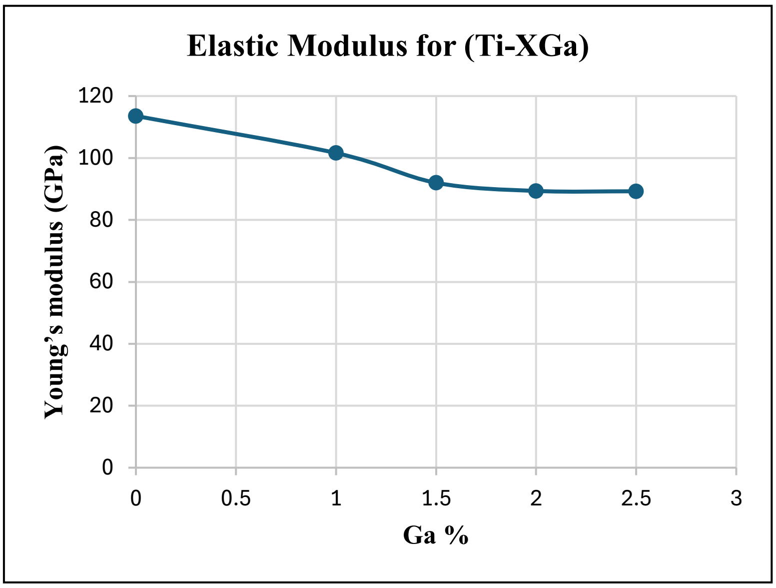

Fig. 18 shows the effect of adding Ga to Ti metal on Young's modulus

3.8. MTT assay results

Cell survival, proliferation, and differentiation at the implant-host tissue interface are crucial during implantation. Titanium and its alloys have excellent biocompatibility and facilitate cell proliferation. Due to the inert surface and the risk of microbial infection, these biometallic alloys must activate their surface to enhance cell contact and inhibit bacterial growth. The cellular response to biomaterial surfaces is considered a fundamental criterion for assessing material biocompatibility.

Fig. 19 shows control untreated MCF-10 cells before being treated with samples.

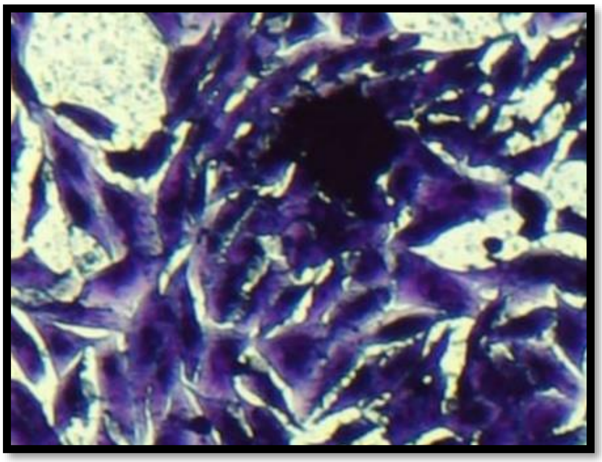

Fig. 19 Control untreated MCF-10 cells (40x)

The antiproliferative activity (anticancer activity) of sample 3 against MCF-10 cells was studied using an MTT assay. As shown in Table 12 and Figs. 20 and 21, the results demonstrate that sample 3 has biocompatibility properties for MCF-10 cells.

Table 12 Cytotoxicity in triplicate of Ti-1.5Ga alloy

Concentration (µg/ml)	Cytotoxicity (%) for A	Cytotoxicity (%) for B	Cytotoxicity (%) for C
0	0	0	0
12.5	3.25	2.35	0.98
25	6.35	5.98	6.35
50	8.36	10.25	7.58
100	11.23	10.54	9.58

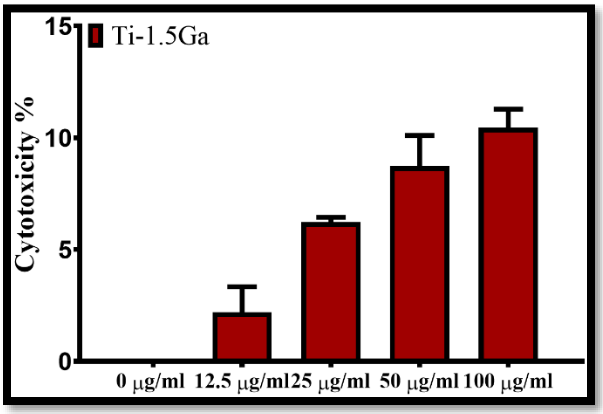

Fig. 20 Cytotoxicity effect of Ti-1.5Ga in MCF-10 cells

The bar chart illustrates the cytotoxic effect (%) of the Ti-1.5Ga alloy on MCF-10 cells at increasing concentrations: 0 ,12.5 ,25,50 ,and 100 µg/ml. At 0 µg/ml (control untreated), cytotoxicity is 0%. As expected, no toxicity was observed without the alloy serving as a baseline. At 12.5 µg/ml, cytotoxicity is ~2%, indicating minimal toxicity at low concentrations and high biocompatibility. At 25 µg/ml, cytotoxicity is ~6%, a Moderate increase but still considered biocompatible (under 10% is often acceptable). At 50 µg/ml, cytotoxicity is ~9%, approaching the threshold where mild cytotoxic effects are observed. At 100 µg/ml, cytotoxicity is ~10.5%, the highest observed cytotoxic effect, but still within a relatively low range of cytotoxicity.

The SEM examination for morphological changes in MCF-10 cells after being treated with Ti-1.5Ga didn't demonstrate any cytotoxic impacts of the samples against MCF-10 cells. It wasn't caused by cell shape changes, cell size reduction, cell clustering, reduced cell extensions, and shrinkage of nuclei, as shown in Fig. 21.

The Ti-1.5Ga alloy shows low to moderate cytotoxicity in MCF-10 cells. It is generally biocompatible up to 50 µg/ml, with slight cytotoxic effects at 100 µg/ml. These results suggest it is a promising biomaterial with good tolerance at low-to-moderate doses, potentially suitable for implantable or biomedical applications.

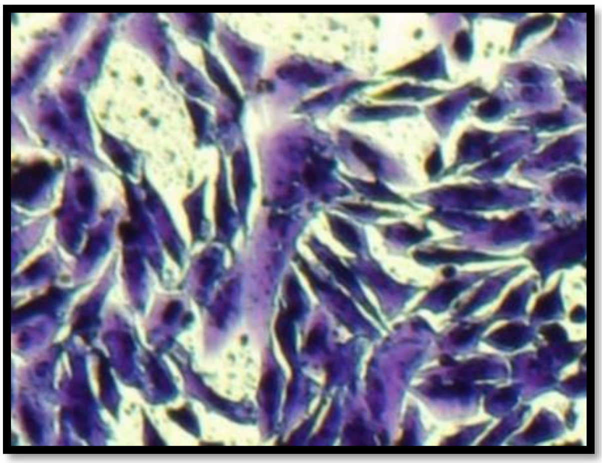

Fig. 21 Morphological changes in MCF-10 cells after being treated with sample 3 (40x)

4. DISCUSSION

Titanium has a larger atomic radius (147 pm) than gallium (135 pm). Lattice shrinkage results from Ga replacing Ti in the hexagonal close-packed (HCP) α-phase lattice when supplied in trace amounts. Nevertheless, even though Ga has a larger atomic mass (69.72 g/mol compared to Ti's 47.87 g/mol), the initial fall in density results from the creation of a disordered solid solution with decreased atomic packing efficiency, which lowers density overall. In a similar form When added in small proportions, Ga substitutes Ti in the α-phase (hexagonal close-packed, HCP) lattice, causing localized lattice contraction and strain. This disrupts atomic packing efficiency, leading to increased porosity due to incomplete densification during sintering. At low Ga levels, the disordered solid solution formation slows atomic diffusion during sintering, reducing interparticle bonding (Wheeler, 2024).

Ga stabilizes metastable α`-phase (hexagonal) or promotes α-phase retention, which inherently has a lower density compared to pure β-phase titanium. This phase stabilization dominates over the atomic mass effect at low concentrations. These phases exhibit irregular atomic arrangements, which can trap pores during solidification. The α`phase in Ti-Ga alloys has a distorted structure that impedes full densification (Cao and He, 2024).

In addition, the alloy transition from α-phase dominance to intermetallic compound formation Ti_3Ga forms. This phase has a tetragonal structure, which is less densely packed than the hexagonal close-packed (HCP) α-phase, leading to a continued density decline (Xiong et al., 2024).

At higher concentrations, intermetallic compound (Ti_3Ga) form. This phase has tighter atomic packing and higher atomic mass contributions, promoting densification. Thus, Ti_3Ga (tetragonal structure) reduces pore connectivity and volume through coherent grain boundaries. At higher Ga levels, Ga segregates at grain boundaries, creating solute-rich regions with higher density, leading to an increase in density. Small Ga additions segregate at grain boundaries, creating solute drag that inhibits pore elimination and Ga enhances dislocation mobility and defect recovery, facilitating pore shrinkage during sintering (Liu et al., 2019).

At low Ga concentrations, Ga reacts with Ti to form intermetallic compound (Ti_3Ga) through metal bonding. This intermetallic compound creates a chemically compatible interface, reducing the contact angle and improving wettability. The reactive wetting process involves Ga diffusing into the Ti substrate, forming a transition layer that lowers interfacial tension (Armbrüster, 2020).

Ga disrupts the native oxide layer on Ti surfaces, which typically inhibits wetting. Small Ga additions reduce oxide stability, allowing direct metal-to-liquid contact and increasing wettability (Fu et al., 2024).

At higher Ga concentrations, thick and brittle intermetallic compound layers (Ti_3Ga) form at the interface. These layers act as diffusion barriers, slowing further reactions and increasing interfacial resistance. The brittleness of intermetallic compound can also lead to spalling, exposing fresh surfaces with decreasing wettability (Chen et al, 2024).

Ga-rich alloys have high surface tension, which counteracts spreading. Additionally, excess Ga promotes rapid re-formation of surface oxides in air, "pinning" the liquid metal and reducing wettability. This is exacerbated by the near-instantaneous oxidation of Ga in ambient conditions (Zhang et al, 2021).

Gallium is a β-phase stabilizer in titanium alloys. Pure Ti at room temperature exists in the hexagonal close-packed (HCP) α-phase, which has a high Young's modulus (~110–120 GPa). However, Ga additions shift the α→β phase transformation temperature, stabilizing the bodycentered cubic (BCC) β-phase, which has a lower modulus (~80–100 GPa) (23. McHendrie et al., 2024).

A study by (Rhianna et al., 2024) found that adding gallium to Ti-Nb alloys can decrease Young's modulus. Research indicates that adding 3% to 5% gallium to a Ti-33Nb matrix can decrease the Young's modulus by 11%.

Sample 3 exhibited higher Antiproliferative activity (anticancer activity) against MCF-10 cells with concentration-dependent cytotoxicity. SEM examination didn't demonstrate any cytotoxic impacts of sample 3 against MCF-10 cells, and wasn't caused by cell shape changes, cell size reduction, cell clustering, reduced cell extensions, and shrinkage of nuclei and have biocompatibility properties (Jasim et al., 2022).

A study by (Al-Shaikhly and Abdul-Baqi, 2023) demonstrated that Incorporating Ga into titanium-silicon alloys significantly improves osseointegration and histological outcomes compared to titanium-silicon alloys and pure titanium. Ti-Si-Ga alloys exhibit superior bone formation, mechanical fixation, and biocompatibility, making them promising candidates for advanced biomedical implant materials.

Another study by (Akman et al., 2023) demonstrated that minor Ga additions (4-8 wt%) to Ti–Nb β-type alloys enhance mechanical strength and corrosion resistance while introducing effective antibacterial properties without cytotoxic effects. The optimized Ga content maintains the desirable β-phase microstructure and low elastic modulus, making these alloys highly suitable for orthopedic implant applications where infection prevention and mechanical compatibility are critical.

5. CONCLUSION

1. The addition of Ga at different concentrations resulted in grain refinement and improved structural distribution of the samples.
2. Adding Ga in different proportions led to the emergence of transformations in the metallic phases and intermetallic compounds. It was observed that it resulted in the emergence of intermetallic compounds such as Ti_5Ga_3 or Ti_3Ga in Ti metal. Also, increased the stability of the α phase.
3. Adding Ga decreased the density of the samples, with the lowest density occurring at 1 wt.% Ga, as it was observed that it reduced the density of Ti metal from (3.9268 g/cm3) to (3.8821 g/cm3) by about (1%).

4. Adding Ga increased the porosity of the samples with the highest porosity occurring at 1 wt.% Ga, as it was observed that it increased the porosity of Ti metal from (12.85 %) to (13.87 %) by about (8%).
5. Adding Ga at different concentrations decreased the wettability of the samples, and it was observed that it increased the contact angle of Ti from (78.83°) to (95.57°) after 10 seconds by about (21%) at 1 wt.% Ga.
6. Adding Ga decreased modulus of elasticity of the samples with the lowest density occurring at 2.5 wt.% Ga, as it was observed that it reduced modulus of elasticity of Ti metal from (113.56 GPa) to (89.25 GPa) by about (21%).
7. Low cytotoxicity to MCF-10 was recorded at low concentrations up to 50 µg/ml and gradually increased with increasing concentration up to 100 µg/ml due to the potential of Ga^{3+} ions release. The increase in Ga led to increased cytotoxicity, but it remained within acceptable limits. This makes all samples promising candidates for biomaterials applications.

6. REFERENCES

Abbass, M.K., Jasim, A.N., Jasim, M., Khashan, K.S. and Issa, M.J. (2020). Improving bio corrosion resistance of the single layer of nano hydroxyapatite and nano YSZ coating on the Ti6Al4V alloy using electrophoretic deposition. Solid State Technology, 63(6), pp.18584–18597.

Abbass, M.K., Khadhim, M.J., Jasim, A.N. and Issa, M.J. (2021). A study of the effect of porosity of bio-active ceramic hydroxyapatite coated by electrophoretic deposition on the Ti6Al4V alloy substrate. Journal of Physics: Conference Series, 1773(1), 012035.

Akman, A., Alberta, L.A., Giraldo-Osorno, P.M., Turner, A.B., Hantusch, M., Palmquist, A. and Gebert, A. (2023). Effect of minor gallium addition on corrosion, passivity, and antibacterial behaviour of novel β-type Ti–Nb alloys. Journal of Materials Research and Technology, 25, pp.4110–4124.

Alberta, L.A., Vishnu, J., Douest, Y., Perrin, K., Trunfio-Sfarghiu, A.M., Courtois, N. and Calin, M. (2023). Tribocorrosion behavior of β-type Ti-Nb-Ga alloys in a physiological solution. Tribology International, 181, 108325.

Alipal, J., Pu’Ad, N.M., Nayan, N.H.M., Sahari, N., Abdullah, H.Z., Idris, M.I. and Lee, T.C. (2021). An updated review on surface functionalisation of titanium and its alloys for implants applications. Materials Today: Proceedings, 42, pp.270–282.

Al-Shaikhly, M.S. and Abdul-Baqi, H.J. (2023). Osseointegration and histological picture of titanium silicon gallium alloy vs. titanium silicon alloy and pure titanium. Al-Rafidain Journal of Medical Sciences, 5, pp.247–256.

Armbrüster, M. (2020). Intermetallic compounds in catalysis – a versatile class of materials meets interesting challenges. Science and Technology of Advanced Materials, 21(1), pp.303–322.

Cao, M.Z. and He, B.B. (2024). A review on deformation mechanisms of metastable β titanium alloys. Journal of Materials Science, 59(32), pp.14981–15016.

Chen, Y., Zhang, H., Wang, B., Huang, J., Zhou, M., Wang, L. and Ji, J. (2024). A review of research on improving wear resistance of titanium alloys. Coatings, 14(7), 786.

Cochis, A., Azzimonti, B., Chiesa, R., Rimondini, L. and Gasik, M. (2019). Metallurgical gallium additions to titanium alloys demonstrate a strong time-increasing antibacterial activity without any cellular toxicity. ACS Biomaterials Science and Engineering, 5(6), pp.2815–2820.

Fortouna, Y., Alberta, L.A., Vishnu, J., Pilz, S., Gebert, A., Lekka, C. and Calin, M. (2023). Effects of Ga on the structural, mechanical and electronic properties of β-Ti-45Nb alloy by experiments and ab initio calculations. Journal of the Mechanical Behavior of Biomedical Materials, 140, 105728.

Fu, Y., Gao, Y., Jiang, W., Xiao, W., Zhao, X. and Ma, C. (2024). A review of deformation mechanisms, compositional design, and development of titanium alloys with transformation-induced plasticity and twinning-induced plasticity effects. Metals, 14(1), 97.

Jasim, A.J., Sulaiman, G.M., Ay, H., Mohammed, S.A., Mohammed, H.A., Jabir, M.S. and Khan, R.A. (2022). Preliminary trials of the gold nanoparticles conjugated chrysin: An assessment of anti-oxidant, anti-microbial, and in vitro cytotoxic activities of a nanoformulated flavonoid. Nanotechnology Reviews, 11(1), pp.2726–2741.

Jasim, A.N., Abbass, M.K., Jasim, M. and Salah, K. (2020). Synthesis, characterization and optimization of electrophoretic deposition (EPD) parameters of YSZ layer on Ti-6Al-4V alloy substrate. IOP Conference Series: Materials Science and Engineering, 745(1), 012082.

Jasim, M., Abbass, M.K., Salah, K. and Jasim, A.N. (2020). Characterization of electrophoretic deposition parameters of nano hydroxyapatite coating on the Ti6Al4V alloy using DC current. AIP Conference Proceedings, 2213(1), 020203.

Jiang, P., Zhang, Y., Hu, R., Shi, B., Zhang, L., Huang, Q. and Lin, C. (2023). Advanced surface engineering of titanium materials for biomedical applications: From static modification to dynamic responsive regulation. Bioactive Materials, 27, pp.15–57.

Liu, S., Zhang, G., Shi, M., Yang, X. and Li, A. (2019). Microstructure and properties of porous titanium prepared by spark plasma sintering. Metals, 9(1), 82.

McHendrie, R., Nguyen, N.H., Nguyen, M.T., Fallahnezhad, K., Vasilev, K., Truong, V.K. and Hashemi, R. (2024). Development of novel antibacterial Ti-Nb-Ga alloys with low stiffness for medical implant applications. Journal of Functional Biomaterials, 15(6), 167.

Naghavi, S.A., Tamaddon, M., Garcia-Souto, P., Moazen, M., Taylor, S., Hua, J. and Liu, C. (2023). A novel hybrid design and modelling of a customised graded Ti-6Al-4V porous hip implant to reduce stress shielding: An experimental and numerical analysis. Frontiers in Bioengineering and Biotechnology, 11, Article number not specified.

Sarraf, M., Rezvani Ghomi, E., Alipour, S., Ramakrishna, S. and Sukiman, N.L. (2022). A state-of-the-art review of the fabrication and characteristics of titanium and its alloys for biomedical applications. Bio-Design and Manufacturing, 5(2), pp.371–395.

Sidhu, S.S., Singh, H. and Gepreel, M.A.H. (2021). A review on alloy design, biological response, and strengthening of β-titanium alloys as biomaterials. Materials Science and Engineering C, 121, 111661.

Vishnu, J., Alberta, L.A., Hariharan, A., Pilz, S., Gebert, A. and Calin, M. (2022). Novel low modulus beta-type Ti–Nb alloys by gallium and copper minor additions for antibacterial implant applications. Journal of Materials Research and Technology, 20, pp.3306–3322.

Wheeler, D.W. (2024). Structure and mechanical properties of a titanium–8 wt.% gallium alloy. Crystals, 14(12), 1061.

Xiong, Y., Liu, Z., Zhao, Z. and Li, B. (2024). Numerical investigation on the evolution behavior of solidification structure in titanium alloy during vacuum arc remelting process. Metallurgical and Materials Transactions B, 55(6), pp.4182–4199.

Zhang, B., Huang, M., Chong, Y., Mao, W., Gong, W., Zheng, R. and Tsuji, N. (2021). Achieving large super-elasticity through changing relative easiness of deformation modes in Ti-Nb-Mo alloy by ultra-grain refinement. Materials Research Letters, 9(5), pp.223–230.

Zhu, S., Zhu, C., Luo, D., Zhang, X. and Zhou, K. (2023). Development of a low-density and high-strength titanium alloy. Metals, 13(2), 251.